Applied Physics Express

LETTER • **OPEN ACCESS**

Probing buried interface band dispersion of a MgO/Fe heterostructure with hard X-ray angle-resolved photoemission

To cite this article: Shigenori Ueda and Masaki Mizuguchi 2024 *Appl. Phys. Express* **17** 075501

OPEN ACCESS

Applied Physics Express 17, 075501 (2024) LETTER

https://doi.org/10.35848/1882-0786/ad5e33

Probing buried interface band dispersion of a MgO/Fe heterostructure with hard X-ray angle-resolved photoemission

Shigenori Ueda[1,2*] and Masaki Mizuguchi[3,4,5,6]

[1]Research Center for Electronic and Optical Materials, National Institute for Materials Science (NIMS), Tsukuba, Ibaraki 305-0044, Japan
[2]Synchotron X-ray Station at SPring-8, NIMS, Sayo, Hyogo 679-5148, Japan
[3]Institute of Materials and Systems for Sustainability, Nagoya University, Nagoya, Aichi 464-8603, Japan
[4]Graduate School of Engineering, Nagoya University, Nagoya, Aichi 464-8603, Japan
[5]Cutting-edge, International Research Units, Nagoya University Institute for Advanced Study, Nagoya University, Nagoya, Aichi 464-8603, Japan
[6]Center for Spintronics Research Network, Osaka University, Toyonaka, Osaka 560-8531, Japan

*E-mail: UEDA.Shigenori@nims.go.jp

Received June 28, 2024; accepted July 1, 2024; published online July 16, 2024

Interface band dispersion of a MgO(2 nm)/Fe(50 nm) heterostructure was detected by hard X-ray angle-resolved photoemission spectroscopy (HARPES) with the excitation photon energy of 3.29 keV by utilizing X-ray total reflection (TR). By subtracting bulk-sensitive band dispersion of the buried Fe(001) obtained by HARPES in the non-TR condition from near-interface-sensitive Fe(001) band dispersion obtained by TR-HARPES, the band-folding of Fe and the O 2*p* -Fe 3*d* hybridization at the heterointerface were clearly unveiled. These results suggest that HARPES can probe not only the bulk band but also the buried interface band of heterojunctions. © 2024 The Author(s). Published on behalf of The Japan Society of Applied Physics by IOP Publishing Ltd

Recently, hard X-ray photoemission spectroscopy (HAXPES) has been developed for the measurements of bulk-sensitive electronic and magnetic states of solids[1–9] owing to a large inelastic mean-free-path of electrons (λ_e) with several-keV inside solids.[10] HAXPES with an angular resolution (HARPES) for the band dispersion measurements of single crystals or epitaxial thin films[11–14] has also been a powerful tool for detecting bulk band dispersion of materials. The band dispersion measurements for epitaxial films covered by thin protection layers (e.g. AlO_x) by using HARPES are very useful since the surface treatment of the samples is not required in many cases. Although the HARPES measurements are limited by the photoemission Debye–Waller factor (DWF), which is a fraction of the momentum-conserved transition,[2,11,13] observations of band dispersion are expected to be possible in many cases at low-temperature and approximately 3 keV photoexcitation conditions.

In the HAXPES experiments combined with X-ray total reflection (TR), it has been reported that the effective λ_e (λ_{eff}) can be tuned by the incidence angle of X-ray (θ_{in}) with respect to the sample surface and that the depth-dependent electronic (and magnetic) states can be obtained.[5,9] It seems that HARPES combined with TR has a capability for exploring band dispersion of heterointerfaces as well as buried layers, while TR-HARPES has not been reported yet. Here, we focused on a MgO/Fe heterojunction to demonstrate the capability of TR-HARPES, since the interfacial electronic states between the MgO and Fe layers in Fe/MgO/Fe tunnel magnetoresistance (TMR) junctions[15] are still important; differences in band dispersion between interfacial and buried bulk Fe layers are present or not. Very recently it has been reported that the TMR ratio of Fe/MgO/Fe-based junctions reaches 631%, which is the highest value in the TMR junctions at room temperature.[16] In this work, we have performed HARPES measurements for a MgO-capped Fe(001) thin film to observe the band dispersion of near-interface and buried Fe layers in TR and non-TR (NTR) conditions, respectively. In the TR-HARPES measurement, a clear band dispersion from the buried Fe(001) film with the enhanced MgO-derived O 2*p* states was found, while the O 2*p* states were quite weak in the NTR-HARPES measurement. We also found that the band-folding of Fe (001) and the formation of the O 2*p*-Fe 3*d* anti-bonding state at the MgO/Fe heterojunction, which were obtained by the subtraction of bulk band dispersion (NTR condition) from near-interface one (TR condition), suggesting the usefulness of the combination of TR- and NTR-HARPES for probing interface electronic band states.

The HARPES measurements for the MgO(2 nm)/Fe (50 nm)/MgO(001) structure at the temperature (T) of 22 K were performed with the excitation photon energy ($h\nu$) of 3.29 keV at the undulator beamline BL15XU of SPring-8.[3,17] The sample growth procedure was described elsewhere.[6] Although we used a helical undulator as a light source, circularly polarized X-rays were converted to horizontal linear polarized X-rays due to the Bragg reflections[18] in a four-bounce Si 111 monochromator, leading to the degree of linear polarization calculated to be ~0.98. The energy and angle of photoelectrons were analyzed and detected by a hemispherical electron analyzer (VG Scienta R4000). The angular resolution of the electron analyzer was ~0.3° in HARPES.[11] The energy resolution was set to 290 meV, and the binding energy (E_B) was calibrated by the Fermi level (E_F) of the Au film. The spot size of X-rays at the sample position was 25 μm (vertical) × 35 μm (horizontal) in FWHM. The experimental geometry was described elsewhere.[3,11] To control λ_{eff} (depth in Fe with respect to the interface), the relationship of $\lambda_{eff} = \lambda_p\lambda_e/(\lambda_p+\lambda_e)$ was used, where λ_p was X-ray attenuation length in Fe and depended on θ_{in}.[5,19] λ_e for Fe was obtained from the TPP-2M equation.[10]

Figure 1(a) shows the Fe 2*p* core-level HAXPES spectra of the MgO(2 nm)/Fe(50 nm) film measured in the TR and NTR conditions. In the TR condition (λ_{eff} ~1.7 nm), θ_{in} was set to the TR critical angle ($\theta_C = 0.817°$) for Fe, which was

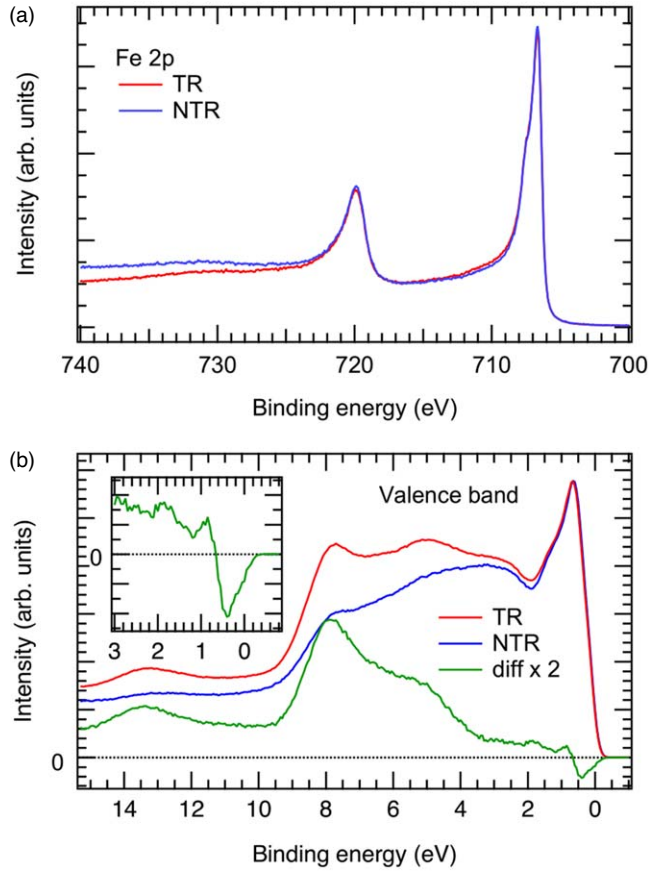

Fig. 1. (a) Fe 2*p* core-level HAXPES spectra of the MgO(2 nm)/Fe (50 nm)/MgO(001) structure measured with the TR (λ_{eff}~1.7 nm) and NTR (λ_{eff}~3.4 nm) conditions at $T = 22$ K. (b) Valence band spectra of the MgO (2 nm)/Fe(50 nm)/MgO(001) structure measured in the TR (λ_{eff}~1.9 nm) and NTR (λ_{eff}~4.0 nm) conditions at $T = 22$ K. The intensity difference between the TR and NTR spectra is indicated by the green line. The inset shows the enlarged view of the difference spectrum around E_F.

detected by the intensity maximum of the Fe 2*p* core-level photoemission as a function of the incidence angle (see Ref. 5 for details), while θ_{in} was set to 2.6° in the NTR condition (λ_{eff} ~3.4 nm). The reduction of the background intensity in the higher E_B side for the TR spectrum compared to the NTR one was found as proof of TR. The similarity of each spectrum indicates that oxidation of Fe near the interface is negligibly weak, since the spectrum obtained in the TR condition is sensitive to the MgO/Fe interface compared to the NTR condition.

Figure 1(b) shows the valence band HAXPES spectra of the MgO(2 nm)/Fe(50 nm) film measured in the TR and NTR conditions, where the spectra have been obtained from the angle-integrated HARPES data shown in Figs. 2(a) and 2(e). Both the TR and NTR spectra (I_{TR} and I_{NTR}) were normalized by the peak intensity at $E_B = 0.65$ eV. The NTR spectrum is roughly classified into two parts: dominant Fe 3*d* states in the E_B range between E_F and ~2 eV and dominant Fe 4*s* states in the range between ~2 and ~9 eV as referred to the previously reported HAXPES spectra for bulk Fe[20] due to the large photoionization cross-section of 4*s* orbital relative to 3*d* one in HAXPES for 3*d* transition metals.[21] For the TR spectrum, additional O 2*p* states originating from the MgO layer are visible in the range between ~4 and ~9 eV according to Ref. 22. A hump structure at around 13 eV is due to carbon contamination on the MgO layer according to Ref. 23. The enhanced MgO-derived states in the TR spectrum is again proof of TR. The intensity difference spectrum (I_{diff}), which is defined by $I_{diff} = I_{TR} - I_{NTR}$, clearly shows the O 2*p* states of MgO in the $E_B > 4$ eV region, while the in-gap of MgO ($E_B < 4$ eV) shows structures, which would reflect the difference in the electronic structures of Fe between the near-interface and bulk regions. In fact, the theoretical calculations for the MgO (001)/Fe(001) multilayer structure indicate that the nearest-neighbor Fe atomic layer from the MgO layer shows the decrease of the density of states (DOS) at around E_F and the increase of DOS at E_B ~2 eV originated from the Fe 3*d* -O 2*p* hybridization at the interface.[6,24] These changes in the electronic structure near the interface are reported in the interface-emphasized HAXPES measurement for the MgO (2 nm)/Fe(1.5 nm)/MgO(001) structure.[6]

Figures 2(a) and 2(e), symbolized by IM_{TR} and IM_{NTR}, respectively, show the HARPES intensity maps for the MgO (2 nm)/Fe(50 nm) film measured in the TR and NTR conditions. Each intensity map was divided by the energy-integrated angular distribution curve (ADC) to partly reduce a detector inhomogeneity along the detector angle. In Fig. 3, the final state wave-vector ($\boldsymbol{k}_f$) passing through the momentum space in the extended Brillouin zone (BZ) for the kinetic energy (E_K) of photoelectrons with 3288 eV excited from E_F for Fe(001) in our experimental geometry is shown. The final state wave-vector corrected by the photon wave-vector ($\boldsymbol{k}_f$—$\boldsymbol{k}_{h\nu}$) is also shown in Fig. 3, since $\boldsymbol{k}_{h\nu}$ cannot be negligible in HARPES as can be seen in the figure. One sees that $\boldsymbol{k}_f$—$\boldsymbol{k}_{h\nu}$ passes through near the Γ–H direction.

Figures 2(b) and 2(f), symbolized by IM_{TR_BG} and IM_{NTR_BG}, respectively, show the intensity maps of the angle-integrated energy distribution curves (EDCs) obtained from Figs. 2(a) and 2(e) with no angular dependence, to assume the non-momentum-conserved transition intensity maps as a background for simplicity. Here, the intensity maps of Figs. 2(a) and 2(b) [Figs. 2(e) and 2(f)] were normalized by their angle-integrated EDCs at $E_B = 0.65$ eV. Figures 2(c) and 2(g), symbolized by IM_{TR_C} and IM_{NTR_C}, respectively, show the HARPES intensity maps for TR and NTR after subtracting the background intensity maps shown in Figs. 2(b) and 2(f). These intensity maps are obtained by $IM_{TR\_C}=IM_{TR} - \alpha\times IM_{TR\_BG}$ and $IM_{NTR\_C} = IM_{NTR} - \beta\times IM_{NTR\_BG}$, where α and β are coefficients. One sees that the clear band dispersion features in Figs. 2(c) and 2(g) compared to those in Figs. 2(a) and 2(e) are apparent. This subtraction process also gives DWF of Fe in our experimental condition. The DWFs given by 1–α for the TR condition and 1–β for the NTR condition for Fe at $T = 22$ K and $E_K = 3288$ eV are ~0.40. This value is close to the calculated DWF of 0.37 based on Refs. 2 and 11. Thus, this subtraction process can roughly estimate DWF from the experimental HARPES results.

Figures 2(d) and 2(h) compare the experimental band dispersion with the theoretical calculation based on the local-spin-density approximation (LSDA).[25] Although the experimentally probed momentum region slightly deviates from the Γ–H direction, the experimental results of both TR and NTR conditions are similar to the LSDA calculations along the Γ–H direction. One sees that the intensity at E_B of ~2 eV

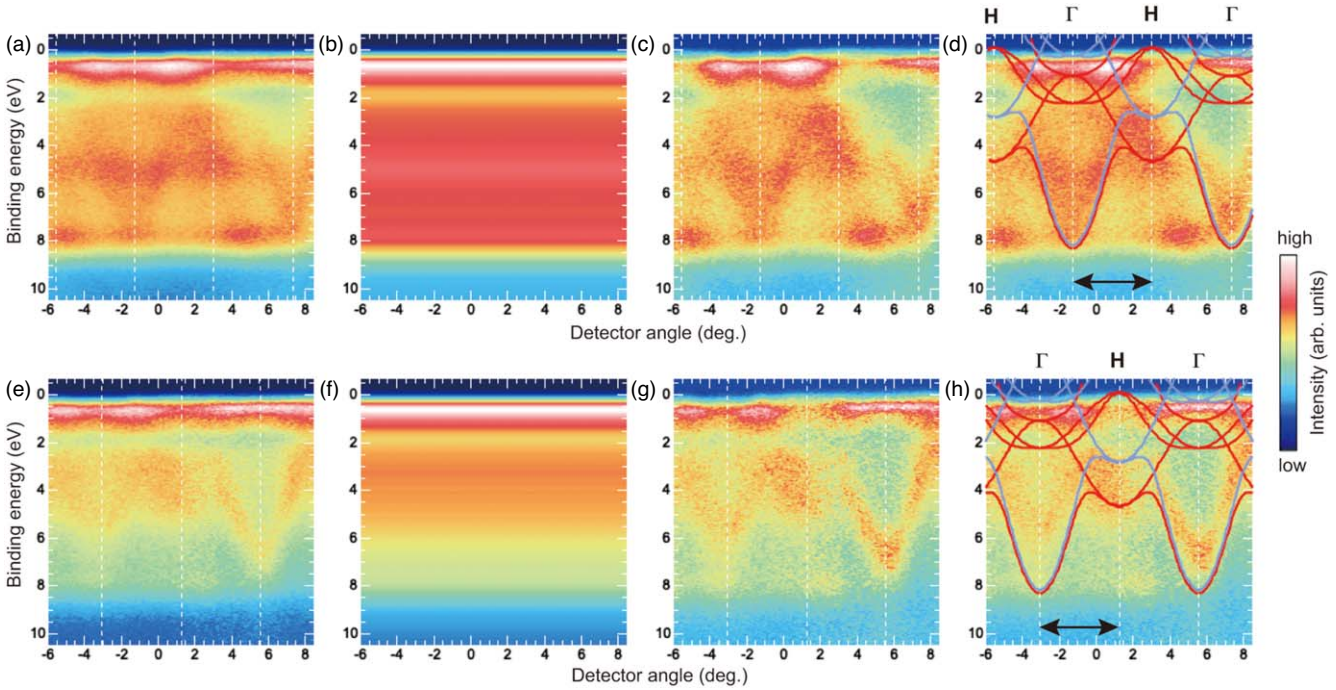

Fig. 2. (a) and (e) Experimental HARPES intensity maps for the MgO(2 nm)/Fe(50 nm)/MgO(001) structure in the TR and NTR conditions, respectively, measured at $T = 22$ K. In the valence band region, λ_{eff} is ∼1.9 (∼4.0) nm in the TR (NTR) condition. (b) and (f) Background intensity map obtained from the angle-integrated EDC in each map. No angular-dependent intensity distribution is assumed. (c) and (g) Corrected HARPES intensity maps for TR and NTR conditions, respectively. (d) and (h) same as (c) and (g), but the theoretical spin-resolved band dispersions along the Γ–H direction are overlaid, where the majority (minority) spin band is indicated by the red (light blue) lines, where the band dispersion data are taken from Ref. 25.

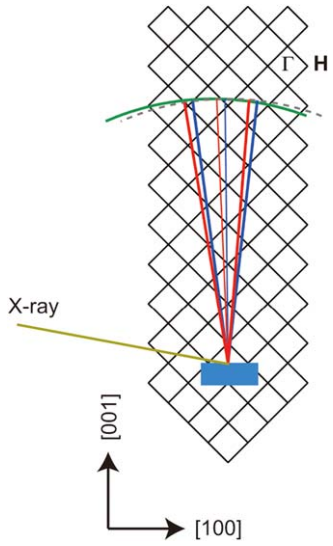

Fig. 3. Extended BZ in HARPES for Fe(001) in our experimental setup. The center (corner) of black squares corresponds to Γ (H) point. The gray dashed and green solid curves correspond to the trace of $\boldsymbol{k}_f$ and $\boldsymbol{k}_f$–$\boldsymbol{k}_{h\nu}$ for $E_{\mathrm{K}} = 3288$ eV, respectively. The red (blue) thick lines indicate the maximum detector field of view for $|\boldsymbol{k}_f$–$\boldsymbol{k}_{h\nu}|$ in the TR (NTR) conditions. The red (blue) thin line indicates the center of the detector field of view in the TR (NTR) conditions.

around the Γ point in the experiment damps in both TR and NTR conditions, while the flat-band-like majority spin band states are present in the calculation. The damping and broadening of the majority spin band has been reported in surface-sensitive spin-resolved ARPES for Fe(110),[26] and the importance of many-body correlation effects in ARPES has been discussed in the theoretical calculations for Fe.[26–30]

To emphasize the interface sensitivity in HARPES, the intensity difference map ($IM_{\mathrm{diff}} = IM_{\mathrm{TR\_C}}$–$IM_{\mathrm{NTR\_C}}$) of the HARPES maps between Figs. 2(d) and 2(h) in the Γ–H region, indicated by black arrows, is shown in Fig. 4(a), where $IM_{\mathrm{TR\_C}}$ and $IM_{\mathrm{NTR\_C}}$ are normalized by their angle-integrated EDCs at $E_{\mathrm{B}} = 0.65$ eV within the Γ–H region. One sees that the negative and positive intensity regions are found even after the subtraction process and that the intensity difference map is antisymmetric to the $\bar{\mathrm{X}}$ point. Here, the positive (negative) intensity mainly arises from the interface (bulk) electronic states. In Fig. 4(b), the difference map was compared with the band dispersion along the Γ–H direction of Fe. The negative intensity area partly agrees with the Δ_1 majority and minority spin band and the majority spin band around the H point at $\sim E_{\mathrm{F}}$, while the positive intensity area does not show a similarity to the band dispersion curves. When we applied the band-folding at the $\bar{\mathrm{X}}$ point as shown in Fig. 4(c), the positive intensity area partly agreed with the folded majority and minority spin band, although the band-folding does not occur in the ideal interface structure for MgO/Fe as described in Ref. 31. The absence of the band-folding in the ideal MgO/Fe interface is due to the in-plane lattice period of Fe is the same as that of MgO at the interface as seen in Fig. 4(d). If oxygen defects at the interface as shown in Fig. 4(e) are present as an example, the in-plane lattice period of Fe is half of that of O-deficient MgO, leading to the band-folding at the $\bar{\mathrm{X}}$ point in Fe at the interface. The O-deficient MgO at the interface might relate to a deposition condition and/or a large lattice mismatch between Fe and MgO and is a possible origin of the band-folding of Fe around the interface. Finally, we note that the intensity integration in the region enclosed by the dashed line at E_{B}

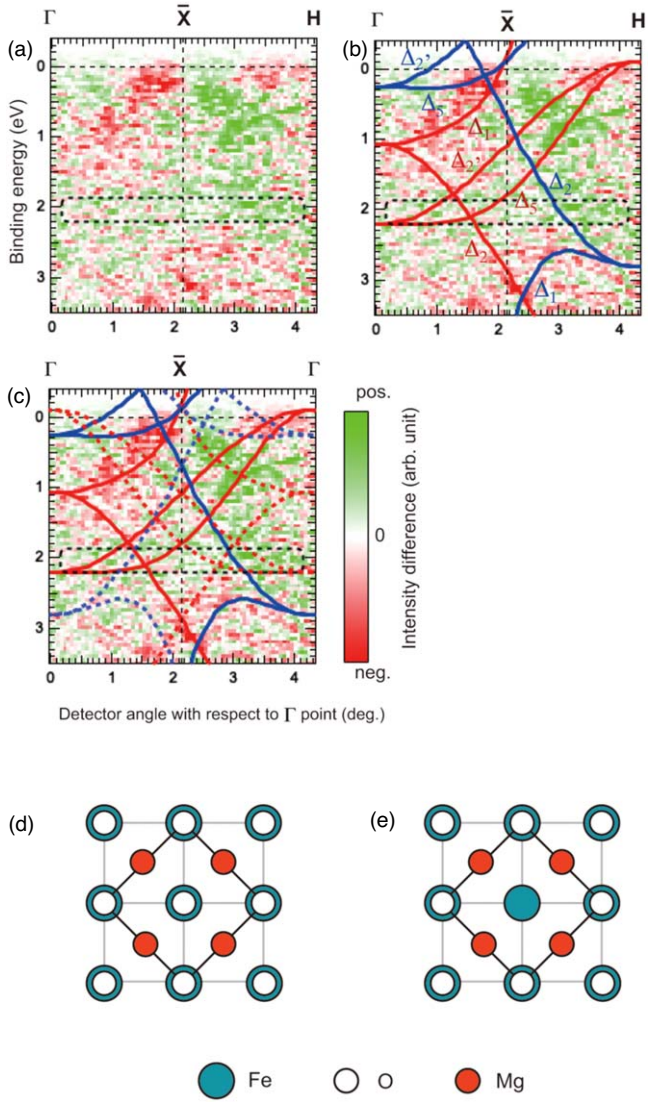

Fig. 4. (a) Intensity difference map obtained by the subtraction of NTR-HARPES [Fig. 2(h)] from TR-HARPES [Fig. 2(d)]. (b) Same as (a), but the spin-resolved band dispersions along the Γ–H direction are overlaid. The red (blue) lines indicate the majority (minority) spin band. (c) Same as (b), but the folding at the $\bar{X}$ point is considered. The folded bands are indicated by the dashed lines. (d) Ideal interface structure of MgO(001)/Fe(001). (e) Same as (d), but O-deficient interface structure.

of ∼2 eV in Fig. 4(a) shows the positive value as similar to the intensity difference spectrum in Fig. 1(b), suggesting that this region is considered to originate from the Fe 3*d*-O 2*p* hybridized states formed at the MgO/Fe interface.[6,24)]

In summary, buried interface band dispersion of the MgO/Fe heterostructure was detected by HARPES combined with the NTR and TR conditions. By subtracting bulk-sensitive band dispersion of the buried Fe(001) obtained by NTR-HARPES from near-interface-sensitive Fe(001) band dispersion obtained by TR-HARPES, the band-folding of Fe and the Fe 3*d*-O 2*p* hybridized state at around the interface were clearly unveiled. These results suggest that HARPES can probe not only the bulk band but also the buried interface band of heterojunctions.

Acknowledgments The HARPES measurements at SPring-8 were performed under the approval of NIMS Synchrotron X-ray Station (Proposal No. 2018B4606). This work was partially supported by Tokodai Institute for Elemental Strategy and Data Creation and Utilization Type Material Research and Development Project from MEXT, Japan [Grant Nos. JPMXP0112101001 and JPMXP1122683430].

ORCID iDs Shigenori Ueda https://orcid.org/0000-0001-9425-0614 Masaki Mizuguchi https://orcid.org/0000-0003-1090-0179

1) S. Hüfner, *Very High Resolution Photoelectron Spectroscopy, Lecture Notes in Physics* (Springer, Berlin, 2007) Vol. 715, Chap.14.
2) C. S. Fadley, J. Electron Spectrosc. Rel. Phenom. **190**, 165 (2013).
3) S. Ueda, J. Electron Spectrosc. Rel. Phenom. **190**, 235 (2013).
4) S. Ueda et al., Appl. Phys. Express **1**, 077003 (2008).
5) S. Ueda, Appl. Phys. Express **11**, 105701 (2018).
6) S. Ueda, M. Mizuguchi, M. Tsujikawa, and M. Shirai, Sci. Technol. Adv. Mater. **20**, 796 (2019).
7) S. Ueda and Y. Sakuraba, Sci. Technol. Adv. Mater. **22**, 317 (2021).
8) S. Ueda, Y. Miura, Y. Fujita, and Y. Sakuraba, Phys. Rev. B **106**, 075101 (2023).
9) S. Ueda, Y. Fujita, and Y. Sakuraba, Phys. Rev. B **109**, 085109 (2024).
10) S. Tanuma, C. J. Powell, and D. R. Penn, Surf. Interf. Anal. **21**, 165 (1994).
11) A. X. Gray et al., Nat. Mater. **10**, 759 (2011).
12) S. Nemšák et al., Nat. Commun. **9**, 3306 (2018).
13) S. Banenkov et al., Commun. Phys. **2**, 107 (2019).
14) S. Chernov, C. Lidig, O. Fedchenko, K. Medjianik, S. Babenkov, D. Vasilyev, M. Jourdan, G. Schönhense, and H. J. Elmers, Phys. Rev. B **103**, 054407 (2021).
15) S. Yuasa and D. D. Djayaprawira, J. Phys. D: Appl. Phys. **40**, R337 (2007).
16) T. Scheike, Z. Wen, H. Sukegawa, and S. Mitani, Appl. Phys. Lett. **112**, 112404 (2023).
17) S. Ueda, Y. Katsuya, M. Tanaka, H. Yoshikawa, Y. Yamashita, S. Ishimaru, Y. Matsushita, and K. Kobayashi, AIP Conf. Proc. **1234**, 403 (2010).
18) T. Ishikawa, K. Tamasaku, and M. Yabashi, Nucl. Instrum. Methods Phys. Res., Sect. A **547**, 42 (2005).
19) B. L. Henke, E. M. Gullikson, and J. C. Davis, At. Data Nucl. Data Tables **54**, 181 (1993).
20) S. Ueda and I. Hamada, J. Phys. Soc. Jpn. **86**, 124706 (2017).
21) M. B. Trzhaskovskaya and V. G. Yarzhemsky, At. Data Nucl. Data Tables **119**, 99 (2018).
22) G. H. Fecher et al., Appl. Phys. Lett. **92**, 193513 (2008).
23) L. H. Tjeng, A. R. Vos, and G. A. Sawatzky, Surf. Sci. **235**, 269 (1990).
24) H. X. Yang, M. Chshiev, B. Dieny, J. H. Lee, A. Manchon, and K. H. Shin, Phys. Rev. B **84**, 054401 (2011).
25) J. Schäfer, M. Hoinkis, E. Rotenberg, P. Blaha, and R. Claessen, Phys. Rev. B **72**, 155115 (2005).
26) J. Sánchez-Barriga et al., Phys. Rev. Lett. **103**, 267203 (2009).
27) A. Grechnev, I. Di Marco, M. I. Katsnelson, A. I. Lichtenstein, J. Wills, and O. Eriksson, Phys. Rev. B **76**, 035107 (2007).
28) J. Minár, J. Phys.: Condens, Matter **23**, 253201.
29) A. L. Walter, J. D. Riley, and O. Rader, New J. Phys. **12**, 013007 (2010).
30) M. C.-T. D. Müller, S. Blügel, and C. Friedrich, Phys. Rev. B **100**, 045130 (2019).
31) K. Nawa, K. Masuda, and Y. Miura, Phys. Rev. Appl. **16**, 044037 (2021).